**J. Cent. South Univ.** (2016) 23: 2809−2817
**DOI:** 10.1007/s11771-016-3344-1

Springer

# Removal of Pb(Π) from aqueous solution by magnetic humic acid/chitosan composites

LIU Yun-guo(刘云国)[1, 2], LI Ting-ting(李婷婷)[1, 2], ZENG Guang-ming(曾光明)[1, 2], ZHENG Bo-hong(郑伯红)[3], XU Wei-hua(徐卫华)[1, 2], LIU Shao-bo(刘少博)[3, 4]

1. College of Environmental Science and Engineering, Hunan University, Changsha 410082, China;
2. Key Laboratory of Environmental Biology and Pollution Control of Ministry of Education (Hunan University), Changsha 410082, China;
3. School of Architecture and Art, Central South University, Changsha 410083, China;
4. School of Metallurgy and Environment, Central South University, Changsha 410083, China



**Abstract:** A novel adsorbent named magnetic humic acid/chitosan composite (M−HA/Cs) was synthesized by decorating humic acid/chitosan composites with $Fe_3O_4$ nanoparticles. The adsorption capacity of M−HA/Cs was 1.5 times that of MCs. The effects of solution pH, initial concentration of Pb(II) ions and adsorption temperature on Pb(II) removal were examined in a batch system and further optimized using Box-Behnken analysis. The recommended optimum conditions are initial Pb(II) concentration of 139.90 mg/L, initial pH of 4.98, and temperature of 43.97 ºC. The adsorption processes could be well described by pseudo-second-order and Elovich models. Isotherm studies reveal that the adsorption process follows Sips and Temkin models. The thermodynamic study indicats that the adsorption process is spontaneous and exothermic. The potential mechanism of Pb(II) on M−HA/Cs at pH 5 may be surface electrostatic attraction, coordination and hydrogen bonding.

**Key words:** chitosan; pollution management; Box-Behnken design; variables optimization; adsorption mechanism

## 1 Introduction

Lead is one of the important pollutants to be removed from wastewaters before migration and transformation into environment because its bad impact on human health and environment security [1−2]. Many technologies, such as chemical precipitation, coagulation, ion exchange and adsorption, have been used to treat lead polluted water. Among these methods, adsorption is one of the most useful and effective techniques for purification of effluents polluted by Pb(II). Several studies have shown that adsorption is a useful and low-cost treatment process if the proper adsorbent is used [3]. Therefore, researchers have focused on searching for naturally materials as cheap and available adsorbents [4].

Chitosan is one of the potential naturally materials due to its low cost and wide availability. It has shown many good properties for its high content of amino and hydroxyl groups. However, chitosan cannot be directly used because of its bad mechanical stability in acidic solutions. Thus, cross-linking or grafted chitosan, like polyaniline grafted chitosan [5], crosslinked alumina-chitosan hybrid adsorbent [6], and chitosan–zeolite composites [7], have been synthesized to improve the mechanical stability, chemical properties and adsorption capacity.

Humic acid (HA), ubiquitous in soil and aquatic environment, plays an important role in the degradation of organic and inorganic pollutants [8]. It can complex with metal ions with the functional groups (like carboxylic acid, methoxyl, alcoholic hydroxyl and ether) bore on the skeleton of alkyl and aromatic units [9]. HA in several physiochemical modifications such as HA coated $SiO_2$ [10], HA coated kaolinite [11], and HA coated $Fe_3O_4$ [8] has been investigated for the removal of metal ions. These studies have indicated that adsorption capacities of adsorbents are enhanced after modified by HA. Thus, humic acid can be chosen to improve the adsorption ability of chitosan. Moreover, separation after adsorption is another important factor of adsorbents. There are several separation methods, such as centrifugation, filtration and magnetic separation. Compared with these methods, magnetic separation is relatively rapid and easy, cost effective and highly efficient. So, chitosan could be magnetized for easy

**Foundation item:** Projects(41271332, 51478470) supported by the National Natural Science Foundation of China
**Received date:** 2015−08−27; **Accepted date:** 2015−11−11
**Corresponding author:** LIU Yun-guo, Professor, PhD; Tel: +86−731−88649208; E-mail: yunguoliu12@163.com

separation [12].

The main objectives of this work are to: 1) synthesize and characterize the magnetic humic acid/chitosan composites (M−HA/Cs) and apply them as adsorbents to remove Pb(II) ions from aqueous solution; 2) investigate the effects of process parameters using Box-Behnken design; 3) study the adsorption mechanism with kinetic, isotherm and thermodynamic models.

## 2 Materials and methods

### 2.1 Materials

Chitosan was supplied by Sinopharm Chemical Reagent. $FeCl_3·6H_2O$, $FeCl_2·4H_2O$, humic acid sodium salts, ammonium hydroxide, glutaraldehyde and $Pb(NO_3)_2$ were purchased from Tianjin Kermel Reagent, China. A stock solution of Pb(II) containing 1000 mg/L was prepared and diluted for the adsorption experiments.

### 2.2 Preparation of materials

Magnetic humic acid/chitosan composites (M−HA/Cs) were prepared by grafting $Fe_3O_4$ onto the surface of humic acid/chitosan composites. Briefly, 2 g $FeCl_2·4H_2O$ and 5.4 g $FeCl_3·6H_2O$ (molar ratio 1:2) were dissolved in distilled water and stirred at 85 ºC, then about 90 mL ammonium hydroxide was added to maintain the solution pH at 10. Magnetic fluid was cooled to room temperature and washed by distilled water. Then 4 g humic acid/chitosan composites with mass ratio of 1:1 are reacted for 48 h to be completely mixed and added to the magnetic fluid at 40 ºC. After that, 50 mL 6.5% glutaraldehyde was injected and then stirred at 60 ºC to form the M−HA/Cs. The obtained M−HA/Cs was washed and finally dried for further usage. Magnetic chitosan (MCs) was prepared as the same procedures except that the humic acid/chitosan composites were replaced by chitosan.

### 2.3 Characteristic of adsorbents

Surface morphology of materials was observed using a scanning electron microscope (SEM Hitachi TM 3000, Japan). The BET specific surface areas and pore diameter of M−HA/Cs were measured by nitrogen adsorption/desorption isotherm method using the automated gas sorption (TriStar II 3020, USA). Fourier transform infrared spectrum (FTIR) was taken using Varian 3100 FTIR (USA). Pb(II) concentration was measured using atomic adsorption spectrometer (PerkinElmer AA700, USA). Stability of HA coating onto M−HA/Cs was studied using UV-vis spectrophotometer (Pgeneral T6, Beijing) at 254 nm. Surface potential of particles were determined by Zeta potential analyzer (ZEN3690, Malvern, UK.).

### 2.4 Batch adsorption experiments

For a typical adsorption experiments, 0.08 g M−HA/Cs was added into 50 mL of Pb(II) solution in Erlenmeyer flasks, and the flasks were agitated at 150 r/min. After adsorption, the mixture was separated by a magnet. The effects of pH (3.0−5.0), Pb(II) concentration (50−150 mg/L), and temperature (15−45 ºC) on adsorption capacity (calculated as Eq. (1)) were investigated by BBD method.

$$q_e = \frac{(C_0 - C_e)V}{m} \tag{1}$$

where $q_e$ is the equilibrium adsorption capacity (mg/g); $C_0$ and $C_e$ are the initial and equilibrium concentration in the solution (mg/L); $V$ is the volume of metal solution (L) and $m$ is the mass of the adsorbent (g).

### 2.5 Box-Behnken design (BBD)

As is known, the solution pH, initial concentration and adsorption temperature have great effects on adsorption process. In order to investigate the effects of the three factors, a 3-level-3-factor BBD experimental design was performed to evaluate and optimize the effects of the three main independent parameters on the Pb(II) adsorption capacity. The solution pH ($X_1$), initial concentration ($X_2$) and adsorption temperature ($X_3$) were set as variable input parameters while adsorption capacity ($Y$) was taken as the response. As shown in Table 1, the factor levels were coded as −1 (low), 0 (central) and 1 (high). The actual experimental design matrix was given in Table 2. The results were analyzed using the correlation coefficient ($R^2$), analysis of variance (ANOVA) and response plots. The experimental data were analyzed by the response surface method with Design-Expert 8.0.0 (Stat-Ease Inc., Minneapolis, MN, USA) and evaluated in the form of quadratic response model Eq.(2).

$$Y = \beta_0 + \sum_{i=1}^{3}\beta_i X_i + \sum_{i=1}^{3}\beta_{ii} X_i^{\,2} + \sum_{i=1}^{2}\sum_{j=2}^{3}\beta_{ij} X_i X_{ij} + \varepsilon \tag{2}$$

where $Y$ is the response value; $\beta_0$, $\beta_i$, $\beta_{ii}$ and $\beta_{ij}$ are the constant, linear, quadratic and interaction coefficient, respectively; $X_i$ and $X_j$ are the levels of the independent variables; $\varepsilon$ is the unanticipated error [13].

**Table 1** Factors used in Box-Behnken experimental design

| Symbol | Factor | Code level | | |
|---|---|---|---|---|
| | | −1 (Low) | 0 (Central) | 1 (High) |
| $X_1$ | pH | 3.0 | 4.0 | 5.0 |
| $X_2$ | Initial concentration/ ($mg·L^{-1}$) | 50 | 100 | 150 |
| $X_3$ | Temperature/ºC | 15 | 30 | 45 |

**Table 2** Experimental and predicted values based on Box-Behnken design (Volume of 50 mL, absorbent dose of 0.08 g, contact time of 24 h and agitation speed of 150 r/min)

| Experiment number | Code variable | | | Response | |
|---|---|---|---|---|---|
| | $X_1$ | $X_2$ | $X_3$ | $Y_{exp}$ | $Y_{pre}$ |
| 1 | 5 | 150 | 30 | 59.73 | 58.93 |
| 2 | 5 | 100 | 45 | 53.01 | 53.85 |
| 3 | 4 | 100 | 30 | 43.55 | 43.67 |
| 4 | 4 | 100 | 30 | 43.38 | 43.67 |
| 5 | 4 | 100 | 30 | 45.10 | 43.67 |
| 6 | 3 | 150 | 30 | 38.61 | 39.5 |
| 7 | 5 | 50 | 30 | 35.87 | 34.98 |
| 8 | 4 | 50 | 15 | 28.61 | 28.65 |
| 9 | 3 | 50 | 30 | 16.08 | 16.89 |
| 10 | 3 | 100 | 15 | 33.65 | 32.81 |
| 11 | 4 | 100 | 30 | 43.70 | 43.67 |
| 12 | 3 | 100 | 45 | 35.58 | 34.72 |
| 13 | 4 | 150 | 45 | 54.25 | 54.21 |
| 14 | 4 | 100 | 30 | 42.64 | 43.67 |
| 15 | 4 | 150 | 15 | 50.27 | 50.22 |
| 16 | 4 | 50 | 45 | 29.19 | 29.22 |
| 17 | 5 | 100 | 15 | 50.36 | 51.21 |

Note: $X_1$ represents pH; $X_2$ represents initial concentration of Pb(II); $X_3$ represents adsorption temperature; $Y_{exp}$ represents experimental values (mg/g); $Y_{pre}$ represents predicted values (mg/g).

### 2.6 Adsorption models of kinetic, isotherm and thermodynamic models

Experimental data obtained from batch experiments were investigated using kinetic isotherm and thermodynamic models. All the model parameters were evaluated by non-linear regression. The optimal model was considered based on correlation coefficient ($R^2$) and root mean square error (RMSE, $E_{rms}$).

## 3 Results and discussion

### 3.1 Characterization of adsorbents

The SEM image, pore size distribution image and FTIR spectra of M−HA/Cs are shown in Fig. 1. The SEM image shows the rough surfaces and small bumps on the surface, indicating the porous structure of M−HA/Cs (Fig. 1(a)). The porous structure is also verified by BET results (Fig. 1(b)). The surface area, average pore size and pore volume are 38.55 $m^2/g$, 6.55 nm and 0.06 $m^3/g$, respectively. These results indicate the poriferous structure of M−HA/Cs may contribute to the transfer of Pb(II) ions to the surface of the adsorbent.

FTIR spectral analysis was employed to confirm the introduction of chitosan, HA and $Fe_3O_4$ in M−HA/Cs and the result is shown in Fig. 1(c). From the spectrum of HA, the characteristic peaks are assigned at 1560 $cm^{-1}$ (C═O stretching of carbonyl group and C—C stretching of

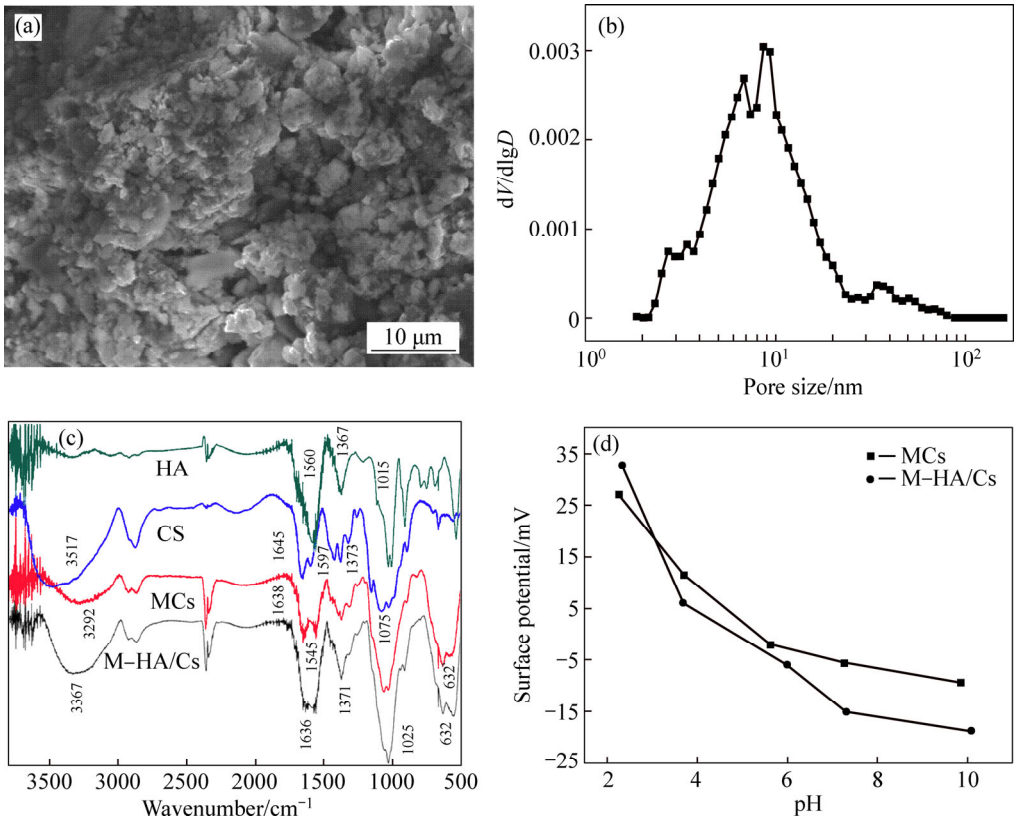


**Fig. 1** Characters of samples: (a) SEM image for M−HA/Cs; (b) Pore size distribution for M−HA/Cs; (c) FTIR spectra for HA, CS, MCs and M−HA/Cs; (d) $pH_{PZC}$ analysis of M−HA/Cs and MCs

aromatic rings), 1367 $cm^{-1}$ (stretching of carbonylate) and 1015 $cm^{-1}$ (C—O band) [14]. As for chitosan, distinctive adsorption peaks are observed as follows: 3517 $cm^{-1}$ (overlapping of N—H and O—H stretching vibration), 1645 $cm^{-1}$ (stretching of amide I), 1579 $cm^{-1}$ (symmetric stretching of amide II), 1373 $cm^{-1}$ (—$CH_3$ symmetric deformation) and 1075 $cm^{-1}$ (C—OH band) [15]. After the modification process, several changes were observed in the spectra of M−HA/Cs and MCs. Firstly, Fe—O bond appears at 632 $cm^{-1}$ on both M−HA/Cs and MCs, indicating the successful wrapped of $Fe_3O_4$. Then, the N−H peak of chitosan at 3517 $cm^{-1}$ shifts to lower frequencies, and the intensity decreases obviously. It indicates that N−H band is involved in the synthesis process. Compared to chitosan, the amide peaks of MCs at 1638 $cm^{-1}$ and 1545 $cm^{-1}$ are shifted and weakened, which is due to the cross-linking reaction between amino group and glutaraldehyde. However, the peaks of M−HA/Cs at 1636 $cm^{-1}$ and 1371 $cm^{-1}$ are dramatically stronger than MCs, even than chitosan, which may be due to the N—H and C═O merging with each other, showing clear indication of the incorporation of HA on M−HA/Cs. Furthermore, the peak of MCs at 3292 $cm^{-1}$ is shifted to 3367 $cm^{-1}$ and intensity increases after HA is involved in M−HA/Cs. The increasing wavenumber and intensity could be attributed to the loaded HA molecules on the surface of M−HA/Cs, which brings a large number of carboxyl and phenol groups, resulting in offsetting the impact of hydrogen bonding [14]. These observations confirm that chitosan, HA and $Fe_3O_4$ have been successfully wrapped in M−HA/Cs.

The stability of HA coated onto M−HA/Cs is tested at pH 2−10, but the dissolution of HA is negligible in the tested pH range. Thus, the stability of M−HA/Cs is suitable for the experiments. Additionally, as shown in Fig. 1(d), the $pH_{pzc}$ values of M−HA/Cs and MCs are 4.8 and 5.4, respectively.

### 3.2 Adsorption capacity comparison between M−HA/Cs and MCs

To investigate the effect of HA on adsorption capacity, M−HA/Cs and MCs are used to remove Pb(II) ions at different pH. The result is shown in Fig. 2. It indicates that the adsorption capacity of the M−HA/Cs is obviously improved after modification. At low pH, both adsorbents show low adsorption capacity due to the strong competition between $Pb^{2+}$ and $H^+$ for the adsorption sites. However, at pH≥4, the adsorption capacity increases by 37% to 50% after modified by HA. This is because the increased number of adsorption sites after modified by HA. As shown at FTIR, the peaks of M−HA/Cs at 3367 $cm^{-1}$, 1636 $cm^{-1}$ and 1371 $cm^{-1}$ are stronger than the corresponding peaks of MCs, indicating more available sites after modification. In addition, the

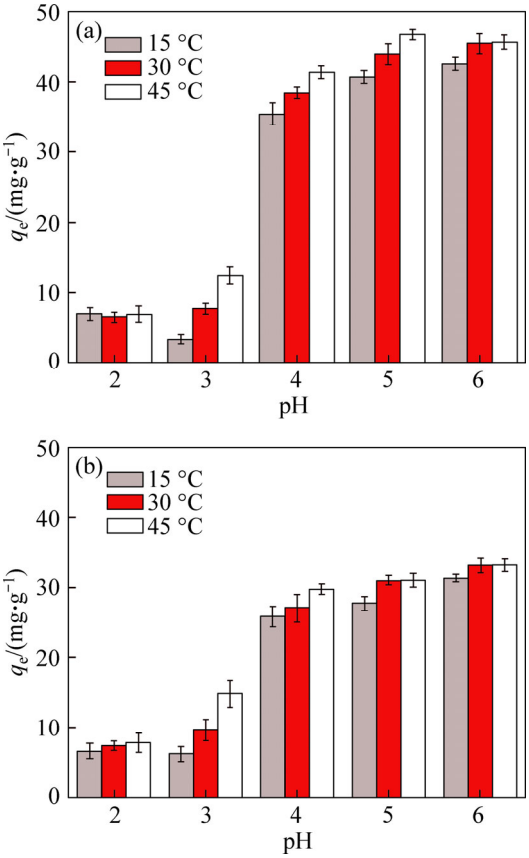


**Fig. 2** Comparison of adsorption capacity between M−HA/Cs (a) and MCs (b)

$pH_{PZC}$ values of M−HA/Cs and MCs are 4.8 and 5.4, respectively. It is indicated that M−HA/Cs has more negative surface, which results in reduced electrostatic repulsion at pH<4.8 and increased electrostatic attraction at pH>4.8. Therefore, the adsorption capacity for Pb(II) is successfully increased after the HA is involved.

### 3.3 Box-Behnken analysis

The BBD, an efficient tool for performing optimization studies with a reasonable number of experimental runs, employs a spherical design with excellent predictability within the design space [16]. To study the effect of pH, initial concentration and temperature, BBD experiments are conducted and the results are shown in Table 1. The result is expressed by a second-order polynomial equation with interaction terms and the final equation in terms of coded factors is

$$Y = 43.67 + 9.38X_1 + 11.64X_2 + 1.14X_3 + 0.33X_1X_2 + 0.18X_1X_3 + 0.86X_2X_3 - 1.76X_1^2 - 4.34X_2^2 + 1.24X_3^2 \quad (3)$$

The ANOVA results for the second-order equation are presented in Table 3. The *F*-value (164.99) implies that the terms in the model have a significant effect on the response. The *p*-value (<0.0001) indicates that the

**Table 3** ANOVA results for quadratic response model

| Source | Sum of squares | d*f* | Mean square | *F*-value | *p*-value |
|---|---|---|---|---|---|
| Model | 1901.42 | 9 | 211.27 | 164.99 | < 0.0001 |
| $X_1$ | 704.09 | 1 | 704.09 | 549.86 | < 0.0001 |
| $X_2$ | 1084.11 | 1 | 1084.11 | 846.64 | < 0.0001 |
| $X_3$ | 10.39 | 1 | 10.39 | 8.11 | 0.0247 |
| $X_1 X_2$ | 0.45 | 1 | 0.45 | 0.35 | 0.5731 |
| $X_1 X_3$ | 0.13 | 1 | 0.13 | 0.1 | 0.7585 |
| $X_2 X_3$ | 2.94 | 1 | 2.94 | 2.29 | 0.1736 |
| $X_1^2$ | 13.09 | 1 | 13.09 | 10.22 | 0.0151 |
| $X_2^2$ | 79.15 | 1 | 79.15 | 61.81 | 0.0001 |
| $X_3^2$ | 6.45 | 1 | 6.45 | 5.03 | 0.0597 |
| Residual | 8.96 | 7 | 1.28 | | |
| Lack of fit | 5.75 | 3 | 1.92 | 2.39 | 0.2099 |
| Pure error | 3.21 | 4 | 0.8 | | |
| $T_m$ | 1910.38 | 16 | | | |
| $D_{Std}$ =1.13 | $R^2$=0.9953 | $R^2_{Adj}$=0.9893 | $R^2_{Pred}$=0.9492 | $P^2_{Adeq}$=48.445 | $C_v$=2.73% |

Note: $T_m$ means totals of all information corrected for mean.

model terms are $D_{Std}$ significant at the 95% of probability level [13, 17]. The *p*-value for lack of fit (0.2099) is found to be non-significant, indicating the validity of the model. The coefficient of variation value ($C_v$=2.73%) shows the precision and reliability of the experiments. Adequate precision (>4) indicates adequate signal to noise [17]. The obtained coefficient (0.9953) and adjusted-$R^2$ (0.9893) indicate high correlation between the observed and the predicted values. The relationship between the actual and predicted values of *Y* is shown in Fig. 3. It can be seen that the quadratic model is adequate because the data points tend to be close to the diagonal line. Thereby, the quadratic model is statistically significant to represent the Pb(II) adsorption by M−HA/Cs.

### 3.4 Effect of various parameters on Pb(II) removal

The ANOVA analysis validates that the linear effects of $X_1$, $X_2$, $X_3$ and quadratic terms of $X_1^2$, $X_1^2$ are significant since the *p*-values are < 0.05 for the factors. To visualize the relationship between the response and operating factors, 3D surface mapping plots are then obtained based on the BBD model. 3D plots performed the relationship between *Y* and two variable factors when the other factor is kept at the central level. The interactive effect of pH and initial concentration at 30 ºC is shown in Fig. 4(a). The convex graph shows the synergistic effect between pH and initial concentration. There are three possible reasons for the synergistic effect: 1) the increasing driving force with temperature enhanced the probability of effective collision between Pb(II) ions and adsorbents; 2) the solution pH significantly affects the speciation of metal ions and the surface charge of the adsorbents [18−19]; 3) electrostatic repulsion turned to electrostatic attraction with the increasing solution pH. The interactive effect of pH and temperature at 100 mg/L is shown in Fig. 4(b). The higher temperature enhances the adsorption capacity of M−HA/Cs due to the decreased solution viscosity and the accelerated diffusing rate of Pb(II) ions [20]. Moreover, the ions distribution in the adsorbent's interspaces and the process of deprotonation reactions were influenced by temperature obviously [21]. Figure 4(c) shows the familiar trend with Figs. 4(a) and (b), which is the interactive effect of initial concentration and temperature.

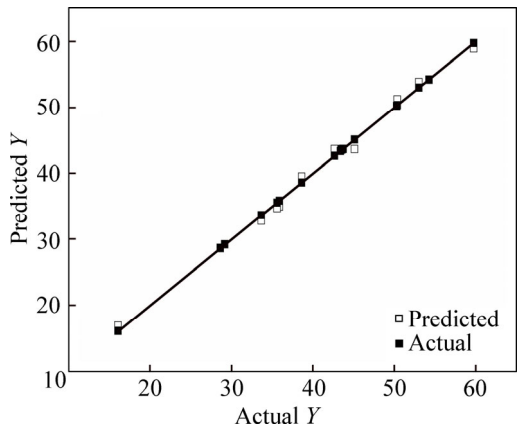


**Fig. 3** Scatter diagram of predicted response versus actual response

Based on the BBD analysis, the maximum adsorption capacity is 60.88 mg/g at optimized conditions: pH of 4.98, initial Pb concentration of 139.90 mg/L and temperature of 43.97 ºC. To investigate the reliability of BBD results, the adsorption experiments

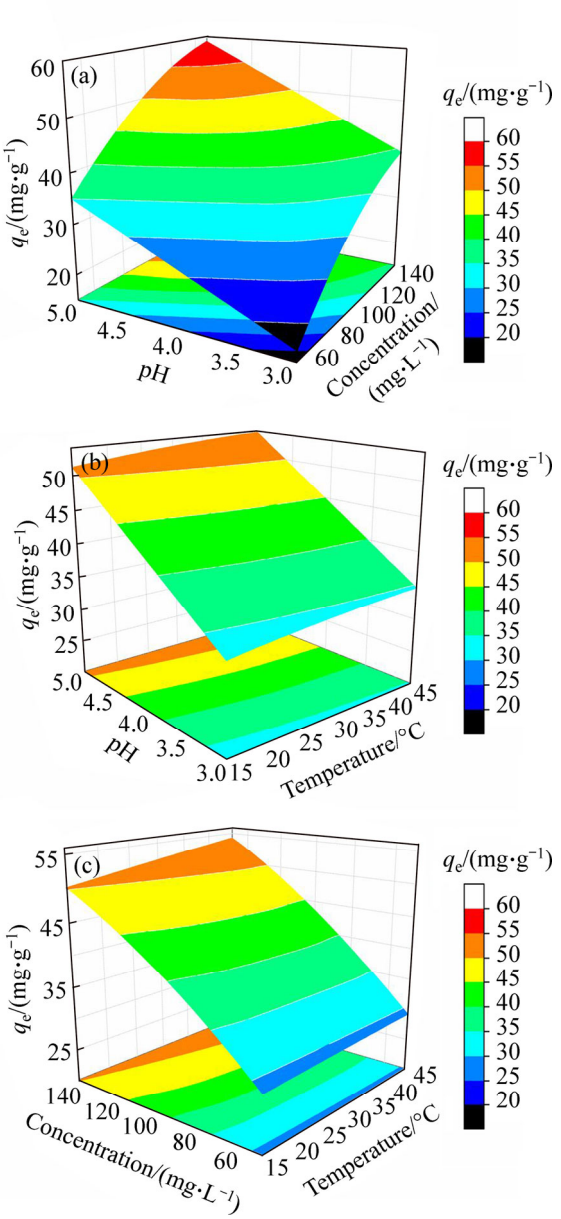


**Fig. 4** 3D surface mapping plots for interactive effect of pH and initial concentration (a), pH and temperature (b), initial concentration and temperature (c)

are conducted under the optimum condition. The adsorption capacity of Pb(II) by M−HA/Cs is 60.38 mg/g, which was in good agreement with the predicted value of 60.88 mg/g, suggesting that the model is reliable in this work.

### 3.5 Adsorption kinetics

In order to explain the mechanism of adsorption processes, pseudo-second-order (Eq. (4)) and Elovich (Eq. (5)) models are applied to simulate the experimental kinetic data.

$$q_t = \frac{q_e^2 k_2 t}{1 + q_e k_2 t} \tag{4}$$

$$q_t = \frac{1}{\beta}\ln(\alpha\beta t + 1) \tag{5}$$

where $q_t$ (mg/g) and $q_e$ (mg/g) are the amounts of adsorption at equilibrium and at time $t$ (min); $k_2$ (g/(mg min)) is the second-order reaction rate equilibrium constant; $\alpha$ (mg/(g·min)) represents the rate of chemisorption at zero coverage; $\beta$ (g/mg) is related to the extent of surface coverage and to the activation energy for the adsorption.

The calculated kinetic results are presented in Fig. 5 and Table 4. It could be seen that the adsorption capacity increases rapidly in the first 90 min and gradually reaches an equilibrium value in 3 h. As shown in Table 4, the experimental data fitted well with the pseudo-second-order and Elovich model, which suggests that the overall rate-limiting step may be the chemisorption process involving valence forces through sharing and/or

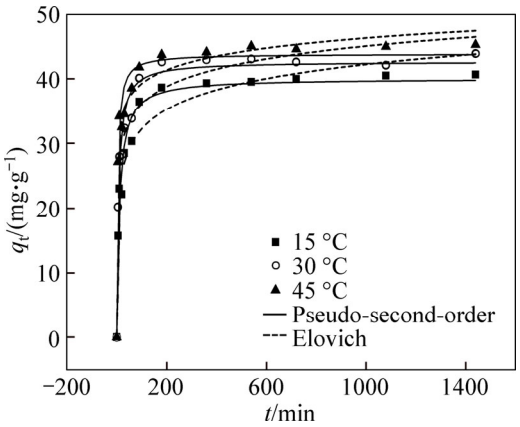


**Fig. 5** Kinetic model plots for adsorption of Pb(II) ions by M−HA/Cs at different temperatures. (Initial concentration of 100 mg/L, volume of 50 mL, absorbent dose of 0.08 g, initial pH of 5 and agitation speed of 150 r/min)

**Table 4** Kinetic parameters for adsorption of Pb(II) ions by M−HA/Cs. (Initial concentration of 100 mg/L, volume of 50 mL, absorbent dose of 0.08 g, initial pH of 5 and agitation speed of 150 r/min)

| Model | Parameter | 15 ℃ | 30 ℃ | 45 ℃ |
|---|---|---|---|---|
| Pseudo-second-order | $q_e$/(mg·g$^{-1}$) | 40.057 | 42.678 | 43.866 |
| | $k_2$/(g·(mg·min)$^{-1}$) | $2.37\times10^{-3}$ | $3.34\times10^{-3}$ | $5.86\times10^{-3}$ |
| | $h$/(g·(mg·min)$^{-1}$) | 3.810 | 6.084 | 9.621 |
| | $R^2$ | 0.967 | 0.968 | 0.962 |
| | RSME | 2.224 | 2.272 | 2.433 |
| Elovich | $\alpha$/(mg·(g·min)$^{-1}$) | 70.912 | 388.340 | 1014 |
| | $\beta$/(g·mg$^{-1}$) | 0.230 | 0.255 | 0.324 |
| | $R^2$ | 0.953 | 0.954 | 0.976 |
| | RSME | 2.675 | 2.729 | 1.954 |
| Exp. | $q_{e,exp}$/(mg·g$^{-1}$) | 40.688 | 43.938 | 45.313 |

ion exchanging [22]. Meanwhile, the highest $h$ and $\beta$ values of Elovich at 45 ºC indicate that the adsorption process easily happens at high temperature.

### 3.6 Adsorption isotherms

The adsorption of Pb(II) ions on M−HA/Cs at different temperatures is investigated by Sips (Eq. (6)) and Temkin (Eq. (7)) isotherm models (Fig. 6). Sips model incorporates three parameters into an equation, which can be applied either in homogeneous or heterogeneous systems. Temkin isotherm model assumes that the heat of sorption of all the molecules in the layer would decrease linearly with coverage due to the sorbate/sorbent interactions [23].

$$q_e = \frac{q_{max} b C_e^n}{1 + b C_e^n} \tag{6}$$

$$q_e = \frac{RT}{b} \ln(K_{Te} C_e) \tag{7}$$

where $q_e$ (mg/g) is the amount of adsorption of Pb(II) at equilibrium; $q_{max}$ (mg/g) is the maximum adsorption capacity of the adsorbent; $b$ is the Sips model constant related to energy of adsorption and $n$ is the Sips model exponent; $K_{Te}$ (L/g) is the equilibrium binding constant; $b$ (kJ/mol) is related to heat of adsorption; $R$ is the gas constant ($8.314\times10^{-3}$ kJ/(K·mol)) and $T$ (K) is the absolute temperature.

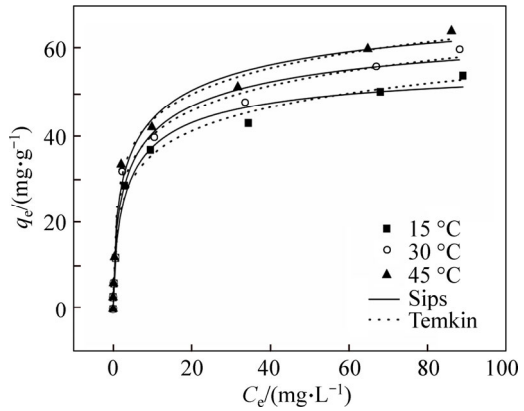


**Fig. 6** Isotherm model plots for adsorption of Pb(II) ions by M−HA/Cs at different temperatures (volume of 50 mL, absorbent dose of 0.08 g, initial pH of 5, contact time of 24 h and agitation speed of 150 r/min)

As can be seen from Table 5, all the $R^2$ values are higher than 0.98, which is due to the good fitting of the experiment data. The values of $n$ are 0.676, 0.567 and 0.539, which indicates that the experimental data are both homogeneous and heterogeneous adsorptions but dominated by the homogeneous adsorption [23]. The $q_{max}$ of Sips models increases with temperature, which indicates that the adsorption of Pb(II) onto M−HA/Cs is more favorable at high temperature. Previous research

**Table 5** Parameters obtained from isotherm models (volume of 50 mL, absorbent dose of 0.08 g, initial pH of 5, contact time of 24 h and agitation speed of 150 r/min)

| Model | Parameters | 15 ºC | 30 ºC | 45 ºC |
|---|---|---|---|---|
| Temkin | $K_{Te}$/(L·g$^{-1}$) | 8.759 | 12.505 | 15.373 |
| | $b_T$/(kJ·mol$^{-1}$) | 0.299 | 0.302 | 0 .304 |
| | $R^2$ | 0.987 | 0.978 | 0.986 |
| | RSME | 2.088 | 3.123 | 2.657 |
| Sips | $q_{max}$/(mg·g$^{-1}$) | 58.078 | 69.945 | 76.312 |
| | $b$/(L·mg$^{-1}$) | 0.386 | 0.378 | 0.397 |
| | $n$ | 0.676 | 0.567 | 0.539 |
| | $R^2$ | 0.986 | 0.981 | 0.984 |
| | RSME | 2.560 | 3.305 | 3.214 |

[24] pointed out that typical bonding energy for ion-exchange mechanism was 8–16 kJ/mol, while physisorption processes was less than −40 kJ/mol. As our $b_T$ of Temkin is not in the two ranges, chemisorption and physisorption may be co-existent in the adsorption process.

### 3.7 Thermodynamics

Thermodynamic parameters are shown in Table 6. The negative values of $\Delta G^0$ confirm the feasibility of the adsorption process and the spontaneous nature of adsorption [25]. The values of $\Delta G^0$ become more negative with the increase of the temperature, indicating more favorable adsorption at higher temperature. The possible interpretation of this trend is that the number of active sites is ascended while the boundary layer surrounding the adsorbent is reduced [26−27]. The positive value of $\Delta H^0$ further confirms the endothermic nature of the adsorption process. The positive $\Delta S^0$ value suggests that some structural changes occur on M-HA/Cs surface, and thus leading to an increase in the disorderness at the M−HA/Cs-water interface [28−29]. As a result, the sorption of Pb(II) on M−HA/Cs is an endothermic and spontaneous process [26, 30]. The results obtained above imply that the adsorption of Pb(II) ions onto M−HA/Cs is an endothermic and spontaneous process.

**Table 6** Thermodynamic parameters for adsorption of Pb(II) ions by M−HA/Cs (volume of 50 mL, absorbent dose of 0.08 g, initial pH of 5 and agitation speed of 150 r/min)

| Temperature/ °C | $\ln K^0$/ (L·mg$^{-1}$) | $\Delta G^0$/ (kJ·mol$^{-1}$) | $\Delta H^0$/ (kJ·mol$^{-1}$) | $\Delta S^0$/ (J·K·mol$^{-1}$) | $R^2$ |
|---|---|---|---|---|---|
| 15 | 2.795 | −6.695 | | | |
| 30 | 3.099 | −7.810 | 12.861 | 67.925 | 0.984 |
| 45 | 3.300 | −8.591 | | | |

### 3.8 Potential mechanism of adsorption

Based on the above discussions, chemisorption and physisorption may be both involved in the adsorption process. Therefore, we proposed the adsorption of Pb(II) onto M−HA/Cs at pH 5 which may be attributed to surface electrostatic attraction, coordination and hydrogen bonding. The potential adsorption patterns of Pb(II) on M−HA/Cs are shown in Fig. 7.

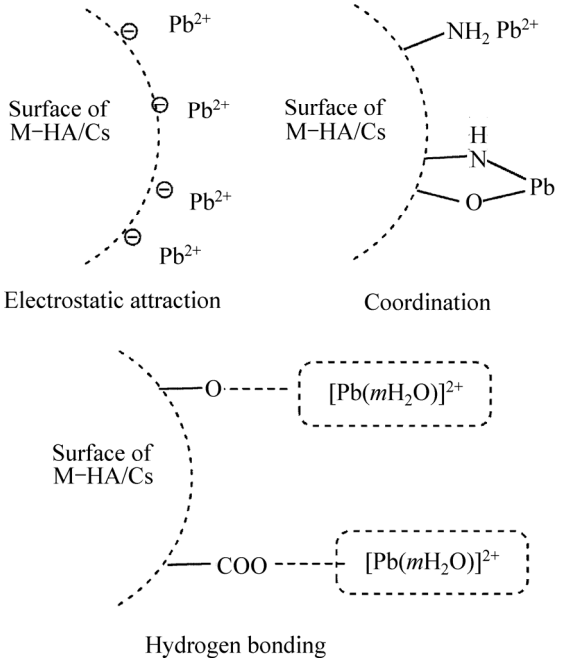


**Fig. 7** Potential adsorption patterns of Pb(II) on M−HA/Cs

The first possible mechanism is electrostatic attraction. As shown in Fig. 8, the predominant Pb(II) species at pH 5 is $Pb^{2+}$ [31]. As the $pH_{pzc}$ of M−HA/Cs is 4.8, the electrostatic attraction happens between the deprotonated surface groups and $Pb^{2+}$. Secondly, the hydroxyl groups and amino groups have lone pairs of electrons for donation, and the $Pb^{2+}$ has vacant orbitals that can accept electron pairs from donor atoms [32]. A lone pair of electrons in the nitrogen atom is donated to

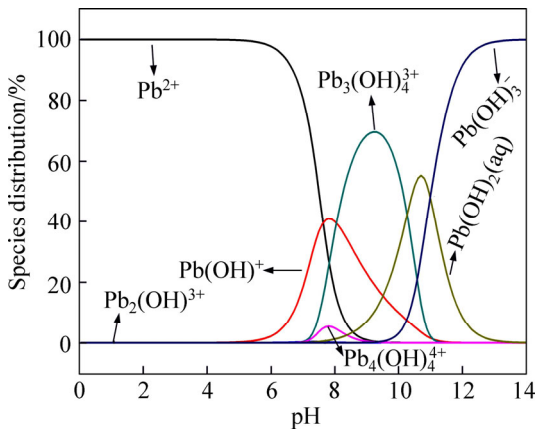


**Fig. 8** Distribution of Pb(II) species in solution as a function of pH computed by the program visual MINTEQ ($C_0$=100 mg/L)

the covalent bond between N and $Pb^{2+}$. In addition, $Pb^{2+}$ attaches itself to two adjacent hydroxyl groups, forming four coordination number compounds and releasing two hydrogen ions into solution [33]. The third possible mechanism may be the interaction between surface groups and hydrated cations by the formation of hydrogen bonding [34−35].

## 4 Conclusions

The M−HA/Cs composites are successfully synthesized and could be easily separated by magnetic separation from the medium after adsorption. The adsorption capacity of M−HA/Cs is 1.5 times higher after modified by HA. The optimum condition obtained from BBD analysis for Pb(II) adsorption is pH 4.98, initial Pb(II) concentration of 139.90 mg/L and temperature of 43.97 ℃. Pb(II) adsorption is influenced by the initial solution pH because pH significantly affects the metal ions speciation and the surface charge of adsorbents. Kinetic studies show that the pseudo-second-order and Elovich model are appropriate to describe the adsorption process. The results illustrated that Pb(II) adsorption is physicochemical process and the chemisorption is the rate-controlling mechanism. The maximum adsorption capacity of M−HA/Cs is 76.31 mg/g. The adsorption is Langmuir-type process and the equilibrium data fit well with Sips and Temkin isotherm models. Parameters from thermodynamic studies show that the adsorption of Pb(II) onto M−HA/Cs is a spontaneous and endothermic reaction. The hypothetical adsorption patterns of Pb(II) on M−HA/Cs may be due to the electrostatic attraction between the negative charged adsorbents surface and Pb(II) species, the ion exchange and the hydrogen boding. Consequently, the experimental results suggest that M−HA/Cs would have broad applications in the removal of Pb(II) ions from aqueous solution.

## References

[1] FAN Qiao-hui, LI Zhan, ZHAO Hao-gui, JIA Ze-hong, XU Jun-zheng, WU Wang-suo. Adsorption of Pb (II) on palygorskite from aqueous solution: Effects of pH, ionic strength and temperature [J]. Applied Clay Science, 2009, 45(3): 111−116.

[2] PAULINO A T, SANTOS L B, NOZAKI J. Removal of $Pb^{2+}$, $Cu^{2+}$, and $Fe^{3+}$ from battery manufacture wastewater by chitosan produced from silkworm chrysalides as a low-cost adsorbent [J]. Reactive and Functional Polymers, 2008, 68(2): 634−642.

[3] TOVAR-GÓMEZ R, MORENO-VIRGEN M R, MORENO-PÉREZ J, BONILLA-PETRICIOLET A, HERNÁNDEZ-MONTOYA V, DURÁN-VALLE C J. Analysis of synergistic and antagonistic adsorption of heavy metals and acid blue 25 on activated carbon from ternary systems [J]. Chemical Engineering Research and Design, 2015, 93: 755−772.

[4] MONIER M. Adsorption of $Hg^{2+}$, $Cu^{2+}$ and $Zn^{2+}$ ions from aqueous

solution using formaldehyde cross-linked modified chitosan-thioglyceraldehyde Schiff's base [J]. International Journal of Biological Macromolecules, 2012, 50(3): 773−781.

[5] KARTHIK R, MEENAKSHI S. Removal of Pb(II) and Cd(II) ions from aqueous solution using polyaniline grafted chitosan [J]. Chemical Engineering Journal, 2015, 263: 168−177.

[6] JI Gui-juan, BAO Wei-wei, GAO Gui-mei, AN Bai-chao, ZOU Hai-feng, GAN Shu-cai. Removal of Cu (II) from aqueous solution using a novel crosslinked alumina-chitosan hybrid adsorbent [J]. Chinese Journal of Chemical Engineering, 2012, 20(4): 641−648.

[7] NGAH W S, TEONG L C, TOH R H, HANAFIAH M A K M. Comparative study on adsorption and desorption of Cu(II) ions by three types of chitosan–zeolite composites [J]. Chemical Engineering Journal, 2013, 223: 231−238.

[8] NIU Hong-yun, ZHANG Di, ZHANG Sheng-xiao, ZHANG Xiao-le, MENG Zhao-fu, CAI Ya-qi. Humic acid coated $Fe_3O_4$ magnetic nanoparticles as highly efficient Fenton-like catalyst for complete mineralization of sulfathiazole [J]. Journal of Hazardous Materials, 2011, 190(1/2/3): 559−565.

[9] LIU Jing-fu, ZHAO Zhong-shan, JIANG Gui-bin. Coating $Fe_3O_4$ magnetic nanoparticles with humic acid for high efficient removal of heavy metals in water [J]. Environment Science & Technology, 2008, 42(18): 6949−6954.

[10] LIANG Liang, LV Ji-tao, LUO Lei, ZHANG Jing, ZHANG Shu-zhen. Influences of surface-coated fulvic and humic acids on the adsorption of metal cations to $SiO_2$ nanoparticles [J]. Colloids Surfaces A, 2011, 389(1/2/3): 27−32.

[11] LU Jia-juan, LI Ying, YAN Xiao-min, SHI Bao-you, WANG Dong-sheng, TANG hong-xiao. sorption of atrazine onto humic acids (HAs) coated nanoparticles [J]. Colloids Surfaces A, 2009, 347(1/2/3): 90−96.

[12] KARA A, DEMIRBEL E, TEKIN N, OSMAN B, BESIRLI N. Magnetic vinylphenyl boronic acid microparticles for Cr(VI) adsorption: Kinetic, isotherm and thermodynamic studies [J]. Journal of Hazardous Materials, 2015, 286: 612−623.

[13] HU Xin-jiang, LIU Yun-guo, WANG Hui, CHEN An-wei, ZENG Guang-ming, LIU Si-mian, GUO Yi-ming, HU Xi, LI Ting-ting, WANG Ya-qin, ZHOU Lu, LIU Shao-heng. Removal of Cu(II) ions from aqueous solution using sulfonated magnetic graphene oxide composite [J]. Separation and Purification Technology, 2013, 108: 189−195.

[14] DONG Chang-long, CHEN Wei, LIU Cheng, LIU Yu, LIU Hai-cheng. Synthesis of magnetic chitosan nanoparticle and its adsorption property for humic acid from aqueous solution [J]. Colloids Surfaces A, 2014, 446: 179−189.

[15] DONG Chang-long, CHEN Wei, LIU Cheng. Preparation of novel magnetic chitosan nanoparticle and its application for removal of humic acid from aqueous solution [J]. Applied Surface Science, 2014, 292: 1067−1076.

[16] KHEMAKHEM B, FENDRI I, DAHECH I, BELGHUITH K, KAMMOUN R, MEJDOUB H. Purification and characterization of a maltogenic amylase from Fenugreek (Trigonella foenum graecum) seeds using the Box Benkhen Design (BBD) [J]. Industrial Crops and Products, 2013, 43: 334−339.

[17] TRIPATHI P, SRIVASTAVA V C, KUMAR A. Optimization of an azo dye batch adsorption parameters using Box–Behnken design [J]. Desalination, 2009, 249: 1273−1279.

[18] SURESHKUMAR M K, DAS D, MARY G, NUWAD J. Adsorption of Pb(II) ions using humic acid coated chitosan-tripolyphosphate (HA-CTPP) beads [J]. Separation Science and Technology, 2013, 48: 1132−1139.

[19] ZHANG Xian, ZHANG Pan-yue, WU Zhen, ZHANG Liang, ZENG Guang-ming, ZHOU Chun-jiao. Adsorption of methylene blue onto humic acid-coated $Fe_3O_4$ nanoparticles [J]. Colloids Surfaces A, 2013, 435: 85−90.

[20] AL-QODAH Z. Adsorption of dyes using shale oil ash [J]. Water Research, 2000, 34(17): 4295−4303.

[21] HO Y, WASE D, FORSTER C. Kinetic studies of competitive heavy metal adsorption by sphagnum moss peat [J]. Environmental Technology, 1996, 17(1): 71−77.

[22] SHEHA R R, EL-ZAHHAR A A. Synthesis of some ferromagnetic composite resins and their metal removal characteristics in aqueous solutions [J]. Journal of Hazardous Materials, 2008, 150: 795−803.

[23] VIJAYARAGHAVAN K, PADMESH T V, PALANIVELU K, VELAN M. Biosorption of nickel(II) ions onto Sargassum wightii: Application of two-parameter and three-parameter isotherm models [J]. Journal of Hazardous Materials, 2006, 133(1/2/3): 304−308.

[24] BILGILI M S. Adsorption of 4-chlorophenol from aqueous solutions by xad-4 resin: Isotherm, kinetic, and thermodynamic analysis [J]. Journal of Hazardous Materials, 2006, 137(1): 157−164.

[25] SINGH T S, PANT K K. Equilibrium, kinetics and thermodynamic studies for adsorption of As(III) on activated alumina [J]. Separation and Purification Technology, 2004, 36: 139−147.

[26] LI Jie, ZHANG Shou-wei, CHEN Chang-lun, ZHAO Gui-xia, YANG Xin, LI Jia-xing, WANG Xiang-he. Removal of Cu(II) and fulvic acid by graphene oxide nanosheets decorated with $Fe_3O_4$ nanoparticles [J]. ACS Applied Materials & Interfaces, 2012, 4(9); 4991−5000.

[27] LI Ting-ting, LIU Yun-guo, PENG Qing-qing, HU Xin-jiang, LIAO Ting, WANG Hui, LU Ming. Removal of lead(II) from aqueous solution with ethylenediamine-modified yeast biomass coated with magnetic chitosan microparticles: Kinetic and equilibrium modeling [J]. Chemical Engineering Journal, 2013, 214: 189−197.

[28] ASFARAM A, FATHI M R, KHODADOUST S, NARAKI M. Removal of Direct Red 12B by garlic peel as a cheap adsorbent: Kinetics, thermodynamic and equilibrium isotherms study of removal [J]. Spectrochim Acta A, 2014, 127: 415−421.

[29] SHENG Guo-dong, DONG Hua-ping, SHEN Run-pu, LI Yi-min. Microscopic insights into the temperature-dependent adsorption of Eu(III) onto titanate nanotubes studied by FTIR, XPS, XAFS and batch technique [J]. Chemical Engineering Journal, 2013, 217: 486−494.

[30] HU Jun, SHAO Da-dong, CHEN Chang-jun, SHENG Guo-dong, REN Xue-mei, WANG Xiang-ke. Removal of 1-naphthylamine from aqueous solution by multiwall carbon nanotubes/iron oxides/ cyclodextrin composite [J]. Journal of Hazardous Materials, 2011, 185(1): 463−471.

[31] LIU Qi, LIU Yong-qiang. Distribution of Pb(II) species in aqueous solutions [J]. Journal of colloid and interface science, 2003, 268: 266−269.

[32] LIU Hui-juan, YANG Fan, ZHENG Yu-ming, KANG Jun, QU Jiu-hui, CHEN J P. Improvement of metal adsorption onto chitosan/Sargassum sp. composite sorbent by an innovative ion-imprint technology [J]. Water Research, 2011, 45(1): 145−154.

[33] BULUT Y, TEZ Z. Removal of heavy metals from aqueous solution by sawdust adsorption [J]. Journal of Environmental Sciences, 2007, 19: 160−166.

[34] HU Xin-jiang, LIU Yun-guo, ZENG Guang-ming, WANG Hui, HU Xi, CHEN An-wei, WANG Ya-qin, GUO Yi-ming, LI Ting-ting, ZHOU Lu, LIU Shao-heng, ZENG Xiao-xia. Effect of aniline on cadmium adsorption by sulfanilic acid-grafted magnetic graphene oxide sheets [J]. Journal of Colloid and Interface Science, 2014, 426: 213−220.

[35] LIU Cheng-bin, WANG Xiao-jian, LIU Rong-hua, WU Yu-lin, LUO Sheng-lian. A new multifunctional polymer: Synthesis and characterization of mPEG-b-PAA-grafted chitosan copolymer [J]. Journal of Central South University of Technology, 2010, 17(5): 936−942.

**(Edited by FANG Jing-hua)**